Science Advances
AAAS

advances.sciencemag.org/cgi/content/full/5/2/eaat7603/DC1

Supplementary Materials for

Human consciousness is supported by dynamic complex patterns of brain signal coordination

A. Demertzi*, E. Tagliazucchi*, S. Dehaene, G. Deco, P. Barttfeld, F. Raimondo, C. Martial, D. Fernández-Espejo, B. Rohaut, H. U. Voss, N. D. Schiff, A. M. Owen, S. Laureys, L. Naccache, J. D. Sitt*

*Corresponding author. Email: a.demertzi@uliege.be (A.D.); Tagliazucchi.enzo@googlemail.com (E.T.); jacobo.sitt@inserm.fr (J.D.S.)

Published 6 February 2019, *Sci. Adv.* **5**, eaat7603 (2019)
DOI: 10.1126/sciadv.aat7603

This PDF file includes:

Supplementary Methods 1

Scanning site effect

In order to rule out potential effects of the recording site on the identified brain patterns, we computed four independent ANOVAs (one for each pattern) with the pattern rate of occurrences as dependent variables, and the patient's clinical condition and scanning site as independent factors. None of the patterns' occurrence probabilities were mediated by scanning site (main effect of scanning site: pattern 1, $F(2,116)=1.5$, $p=0.22$; pattern 2, $F(2,116)=1.2$, $p=0.3$; pattern 3, $F(2,116)=0.99$, $p=0.4$; pattern 4, $F(2,116)=0.21$, $p=0.8$). There was a significant main effect of the clinical condition on the occurrence probabilities for pattern 1 ($F(2,116)=40$, $p<10^{-13}$), pattern 2 ($F(2,116)=3.6$, $p<0.03$) and pattern 4 ($F(2,116)=24$, $p<10^{-8}$) but not for pattern 3 ($F(2,116)=0.84$, $p=0.4$). However, the scanning site × clinical condition interaction was not significant for any of the patterns (pattern 1, $F(4,116)=1.3$, $p=0.28$; pattern 2, $F(4,116)=0.82$, $p=0.99$; pattern 3, $F(4,116)=1.1$, $p=0.4$; pattern 4, $F(4,116)=0.08$, $p=0.52$). These results confirm the absence of a main effect due to the scanning site and the absence of an interaction between clinical condition and scanning site.

Supplementary Methods 2

Pattern characterization with graph theory markers

To better characterize the identified patterns, a quantitative description by means of graph theory metrics was performed to reveal complexity that might not have been evident from the estimated coordination matrices. We estimated the patterns' spatial complexity, weighted edged physical distance, modularity, efficiency, and their capacity for information flow (integration, segregation). A bootstrapping procedure (10.000 repetitions) was implemented to obtain a median and confidence value for each metric. In each repetition a phase coherence matrix was computed from the median of a random sampling of 3033 of images corresponding to each brain pattern in dataset 1. The sampling number (3033) was chosen as the 75% of the images corresponding to the pattern with the smallest representation.

The spatial complexity of the patterns was estimated from the variance and entropy of the distribution of edge weights (fig. S2 A-D). Entropy was calculated by transforming the distribution of values into probability distributions and then applying Shannon's formula, thus a higher entropy reflects a more uniform distribution of edge weights. The procedure was computed in 1 dimension (transforming the whole matrix into a single distribution) and 2 dimensions (using

a sliding kernel of 11x11 elements and averaging the result for each kernel position). The relative distribution of the sum of positive / negative weights across patterns is displayed in fig. S2 E-F.

The characteristic physical brain distance (fig. S2H) of each pattern was estimated from the average of the product of each edge weight (after taking its absolute value) by their respective euclidean distance (normalized by the maximum value).

Efficiency was calculated based on the path length: high global efficiency suggests short mean path lengths, so that the information transfer can occur in parallel and more efficient processes. We computed the efficiency associated to each pattern from the corresponding matrices (after taking absolute values) applying the *efficiency_wei* command from the Brain Connectivity Toolbox (BCT) (fig. S2 K).

The network modularity (Q) quantifies how well the network can be partitioned into communities or modules that maximize the proportion of intra-community edges and minimizes the proportion of inter-community edges. We computed the community structure and the associated modularity value of the weighted signed networks that correspond to each of the coordination patterns. This was performed applying the *community_louvain* function in BCT (fig. S2 L).

Two related measures, integration and segregation, were calculated using the metrics proposed by Deco et al. Integration was defined as the size of the largest component in the matrix corresponding to each pattern. Segregation was defined as the size of the largest component in the matrix corresponding to the number of independent components. The components were obtained after identifying the corresponding connected nodes in the matrix. Note that we considered absolute values because our analysis accounted for communication between the nodes, independently of whether the coupling was positive or negative. To obtain a measure independent of the chosen threshold, the final result followed from computing the integral of this curve in the range of the thresholds between 0 and 1. (fig. S2 I-J).

Finally, to estimate the network properties in relation to conscious states, for each individual the respective probability of each brain pattern was multiplied by the associated median of the corresponding metric. This procedure yielded weighted average values of the network properties for each individual. The results are summarized in fig. S3.

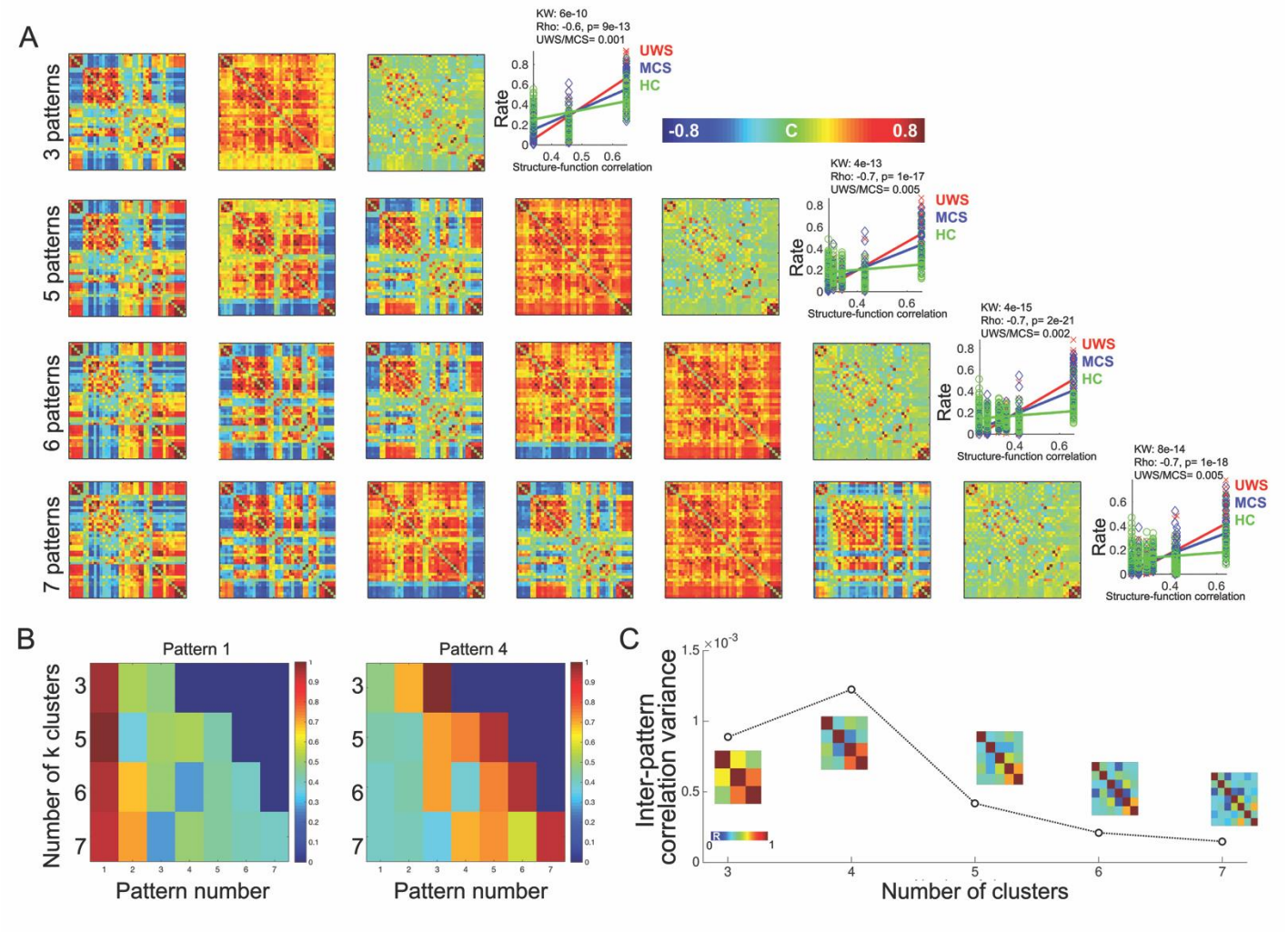

Fig. S1. The four recurrent dynamic coordination patterns emerge at different dimensionalities. (**A**) ***Left****:* Dynamic functional coordination patterns obtained from Dataset 1 using k=3, 5, 6 and 7 number of clusters in the k-means algorithm. For each value of k, patterns are ordered based on their similarity to underlying anatomical connectivity, from the least (left) to the most similar (right). ***Right***: Probability of each pattern's occurrence as a function of their similarity to the structural connectivity matrix for each k-means cluster size. The rate versus coherence-structure relationship is weak for healthy control individuals (green), suggesting a diversity of dynamic changes in typical wakeful conditions. The increased rate versus coherence-structure slope in patients (red, blue) suggests that spontaneous neuronal activity mostly traces the fixed network defined by structural connectivity. (**B**) Left panel shows the similarity of pattern 1 for k=4 with respect to all pattern obtained for k=3 to 7. Right panel presents a similar analysis for pattern 4. These results show an equivalence across the first and the last patterns obtained for different k-values. The fact that these patterns are the main source of distinction between clinical conditions suggest that the main results of our work are robust against variations in the k parameter. (**C**) The variability of dynamic coordination patterns found by the clustering procedure is maximal with k=4 clusters. For each selection of number of clusters in the k-

means algorithm, we computed the correlation matrices between all the upper triangular parts of the resulting centroids. These are the correlation matrices shown next to the symbols, which indicate the variance of their entries. The peak of the variance was found at k=4 clusters, indicating that this choice of the parameter for the k-means algorithm results in the highest variability of the patterns. For smaller k values, distinct patterns appear merged into a single one, while for larger k values repeated patterns appear, thus diminishing the variance.

Notes: The patterns are ordered based on their similarity to underlying anatomical connectivity, from the least (left) to the most similar (right). HC: healthy controls, UWS: unresponsive wakefulness syndrome, MCS: minimally conscious state; p_{KW} = Kruskal-Wallis test p-value, Rho= Spearman rank correlation between the rate and group, UWS/MCS p= Wilcoxon test p-value for the MCS/UWS comparisons, C= coherence.

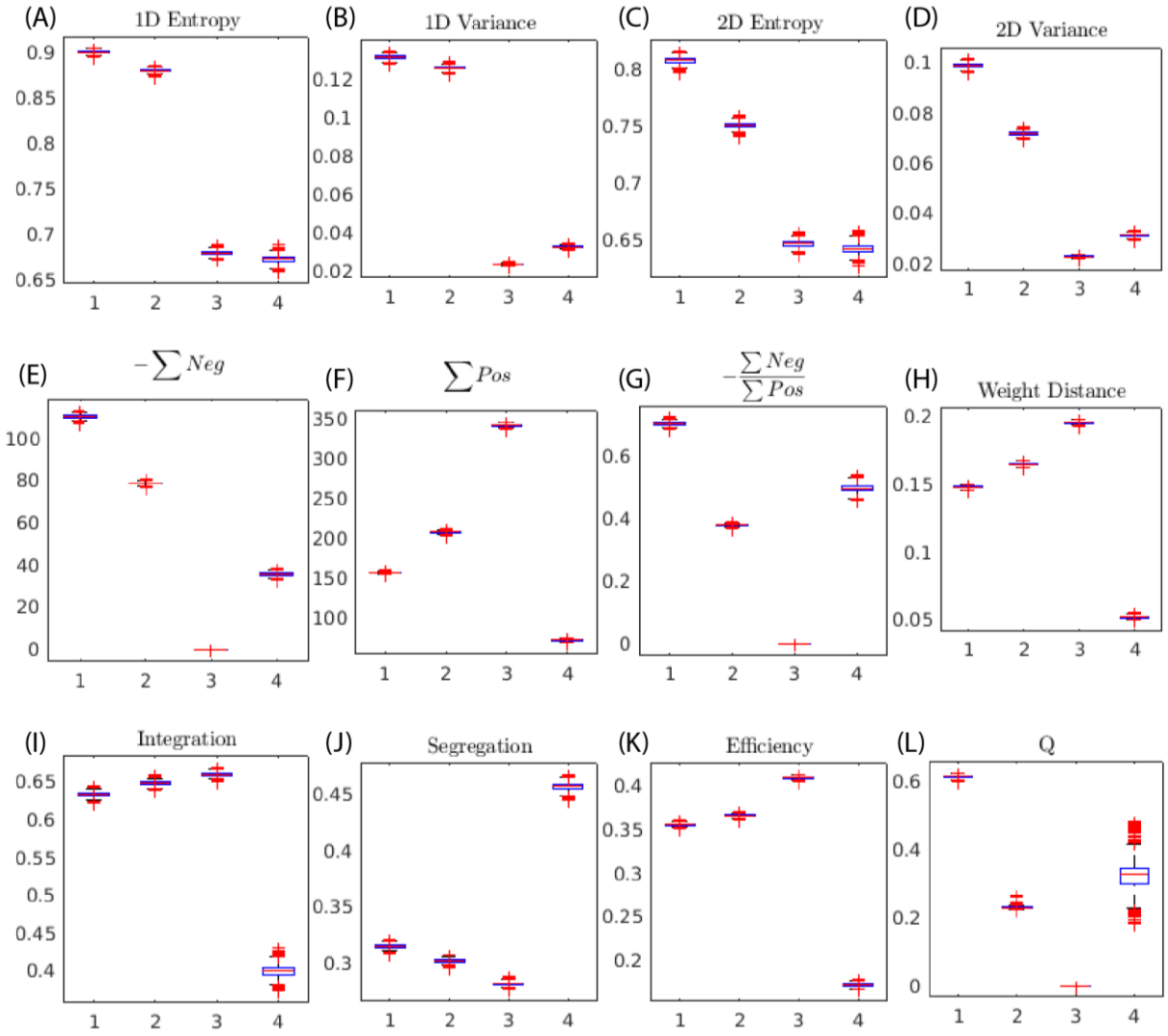

Fig. S2. Network analysis of the identified patterns shows that consciousness-related patterns are characterized by higher spatial complexity, long-distance negative edges, community structure, and high efficiency. A quantitative description by means of graph theory metrics was performed to reveal underlying complexity that may not be evident from the direct observation of the coordination patterns. The patterns' spatial complexity (entropy, variance in one and two dimensions) decreased with the pattern index, from the most complex pattern 1 to the least complex pattern 4 (**A**-**D**). Patterns 1 and 2 were characterized by a large proportion of negative links, with pattern 1 presenting the highest negative/positive ratio (**E**-**G**). Pattern 4 showed smaller average weighted physical distances (**H**), smaller integration (**I**), larger segregation (**J**) and smaller efficiency (**K**) than all the other patterns. (**L**) In contrast, pattern 1 was characterized by the highest modularity and hence by the presence of a community structure

which, in combination with the other metrics, supports that this pattern represents a complex and information-efficient transient organization of whole-brain functional coordination.

Notes: Boxplots represent medians with interquartile range and maximum-minimum values.

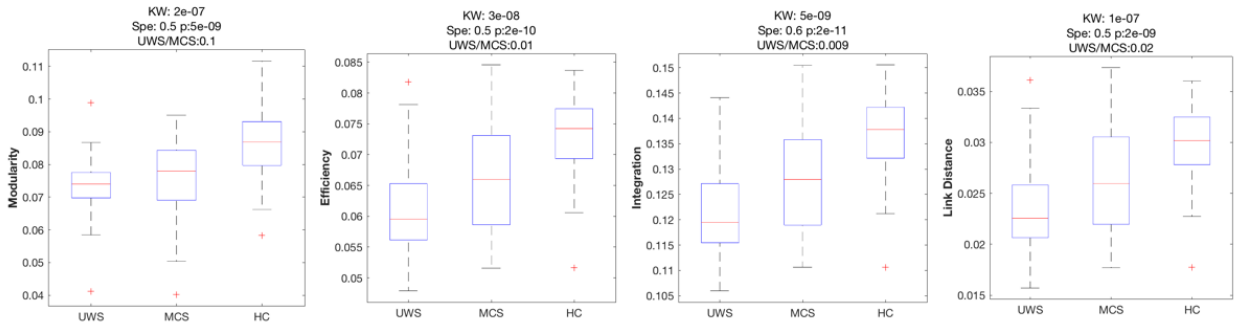

Fig. S3. Network properties reflect the state of consciousness. For each participant, we computed the weighted average modularity (**A**), efficiency (**B**), integration (**C**) and weighted link distance (**D**). The participant-specific measures were computed as the sum of the product of the each one's pattern probability by the median value of each graph-measure. All measures presented increased values with respect to the state of consciousness, with efficiency, integration and distance showing significantly higher values in patients in a minimally conscious state (MCS) as compared to patients in unresponsive wakefulness syndrome/vegetative state (UWS).

Notes: HC: healthy controls. Boxplots represent medians with interquartile range and maximum-minimum values (whiskers). KW = Kruskal-Wallis test, Spe = Spearman rank correlation.

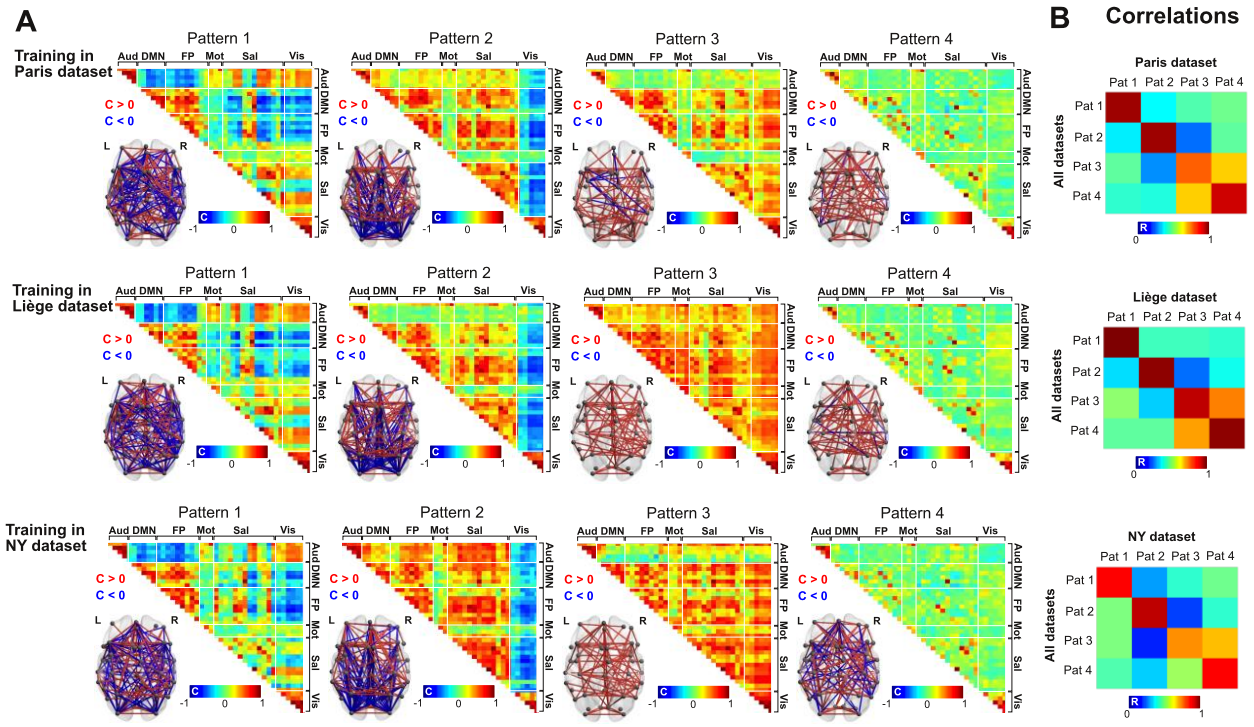

Fig. S4. Robustness of the extracted coordination patterns. (**A**) Clustering of phase-based coherence was estimated separately for the three scanning sites and revealed the emergence of the same coordination patterns as in the main analysis performed on the combined data of all sites together. (**B**) Correlation between phase-based coordination values extracted from the site-specific patterns and the analysis performed using the combined data of all sites. Note that in all cases the index of the most similar pattern is the same in the site-specific and combined-site analysis (diagonal in the matrix).

Notes: (A) The patterns are ordered based on their similarity to underlying anatomical connectivity, from the least (left) to the most similar (right). Brain rendered networks (transverse view) show the top 10% links among regions of interest, with the absolute value of C > 0.2; positive/negative edges indicate positive/negative coherence. Network abbreviations: Aud = auditory, DMN = default mode network, FP = frontoparietal, Mot = motor, Sal = salience, Vis = visual.

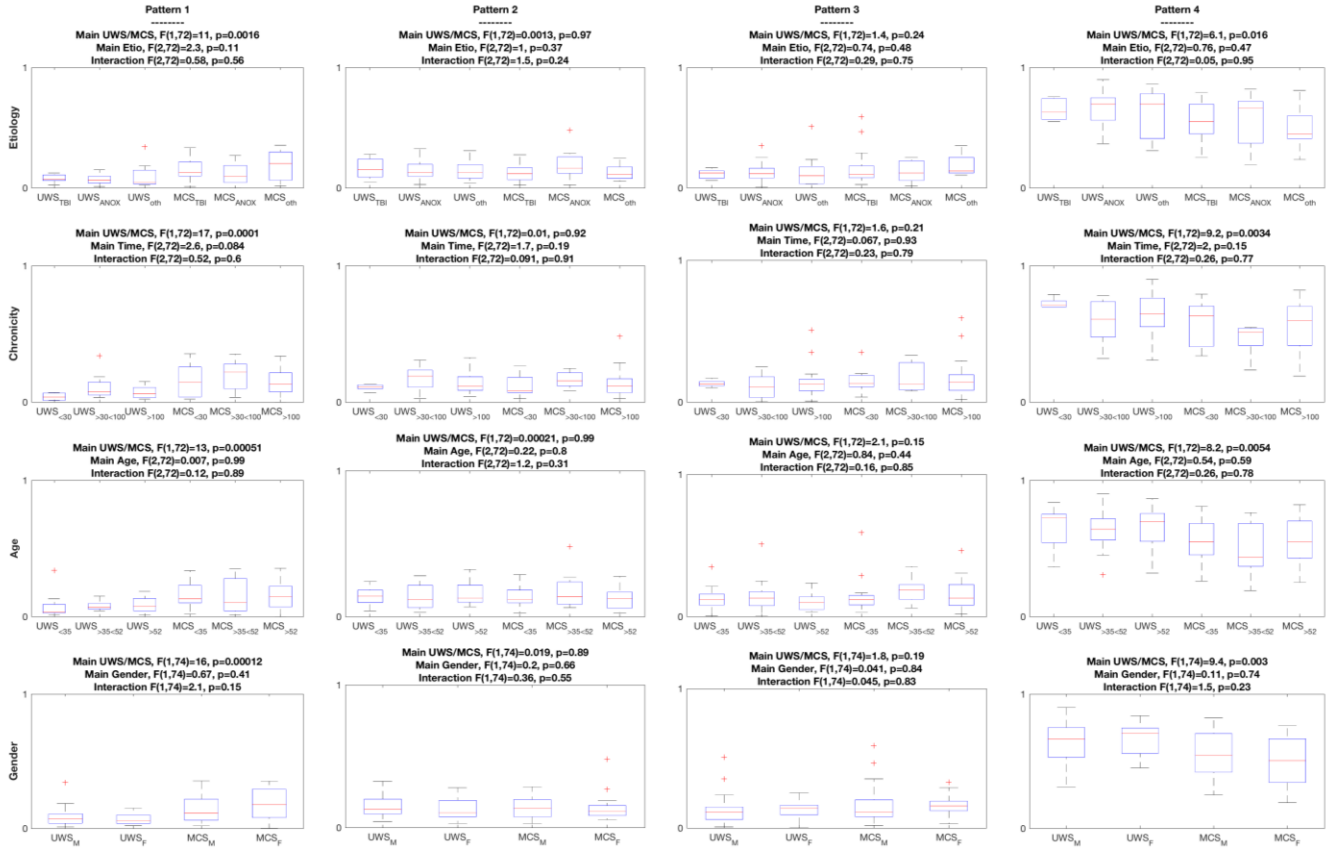

Fig. S5. Etiology, chronicity age, and gender do not mediate patients' temporal dynamics. Across all sites, patients do not differ with respect to how likely the coordination patterns are to occur in each group as a function of etiology, chronicity, age and gender. Main effects were significant only in terms of clinical group, with patients in minimally conscious state (MCS) showing higher occurrence probabilities for pattern 1 and lower rates for pattern 4 as compared to patients in unresponsive wakefulness syndrome (UWS). None of the quantified interactions was significant.

Notes: TBI: traumatic brain injury (8UWS, 17MCS), ANOX: anoxia (21UWS, 11MCS), oth: other etiologies (7UWS, 14MCS). Chronicity, time since injury acute: <30 days (6UWS, 7MCS), subacute 30-100 days (12UWS, 8MCS), chronic: >100 days (18UWS, 27MCS). Age: <35y (12UWS, 15MCS), 35-52y (13UWS, 12MCS), >52y (11UWS, 15MCS). Gender, F: females (12UWS, 14MCS), M: males (24UWS, 28MCS).

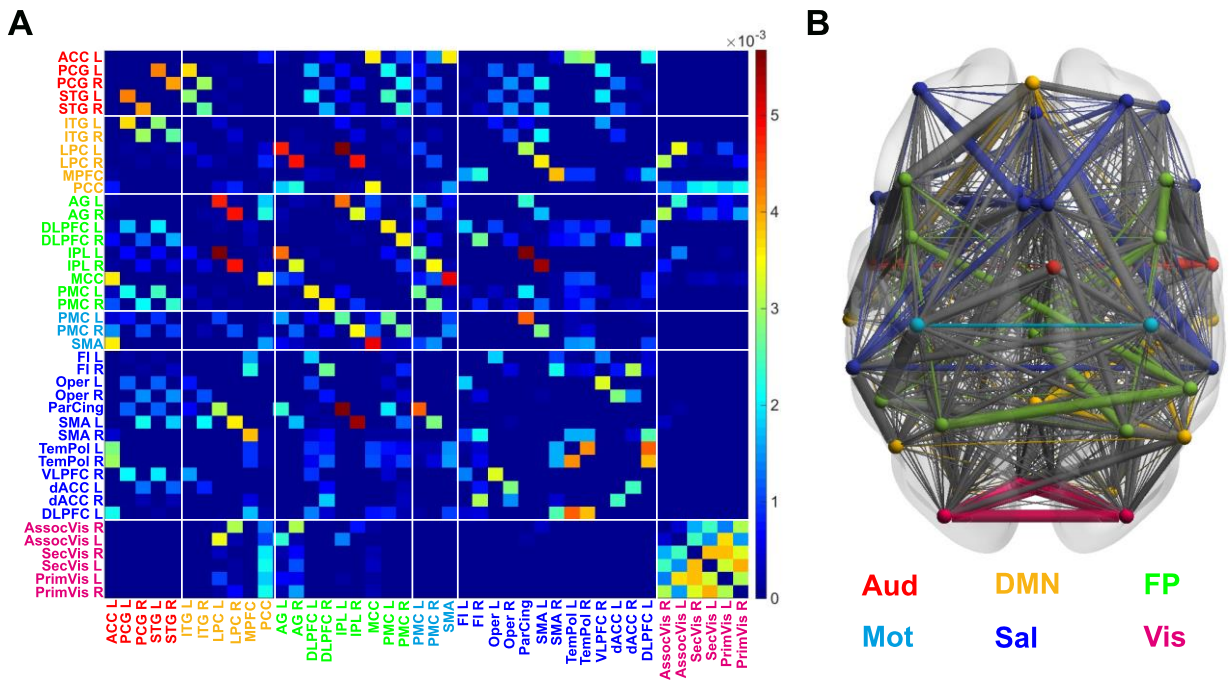

Fig. S6. The structural connectivity network is defined from DSI and contains systems-based ROIs. (**A**) Network of DSI structural connectivity between the 42 regions of interest (ROIs) used in the main analysis. To downsample the network, we considered 30mm spheres centered at each ROI, and computed the mean structural connectivity between all of the original 998 regions within each pair of spheres. (**B**) Network representation of the resampled structural connectivity network rendered on top of a smoothed cortical surface. Only the top 50% connections are shown. Each node represents one of the 42 ROIs. Nodes and within-network connections are colored according to the labels of each network, and between-network connections appear in grey. Before determining this choice of ROIs, we evaluated several parcellation schemes. Brain parcellations were attempted using atlases of the cerebral cortex into 7 and 17 networks in FreeSurfer surface space and MNI152, the Anatomical Labeling (AAL) atlas including 116 cortical and subcortical sphere-ROIs. The network-level atlases time series extraction was successful for the pilot data from controls but was compromised as a result of algorithm failure during the time series extraction for some patients. FreeSurfer, for example, failed at the level of reconstruction for some UWS patients, as also recently shown by Annen and colleagues.

Notes: Network abbreviations Aud: Auditory, DMN: default mode network, FP: frontoparietal, Mot: motor, Sal: salience, Vis: Visual.

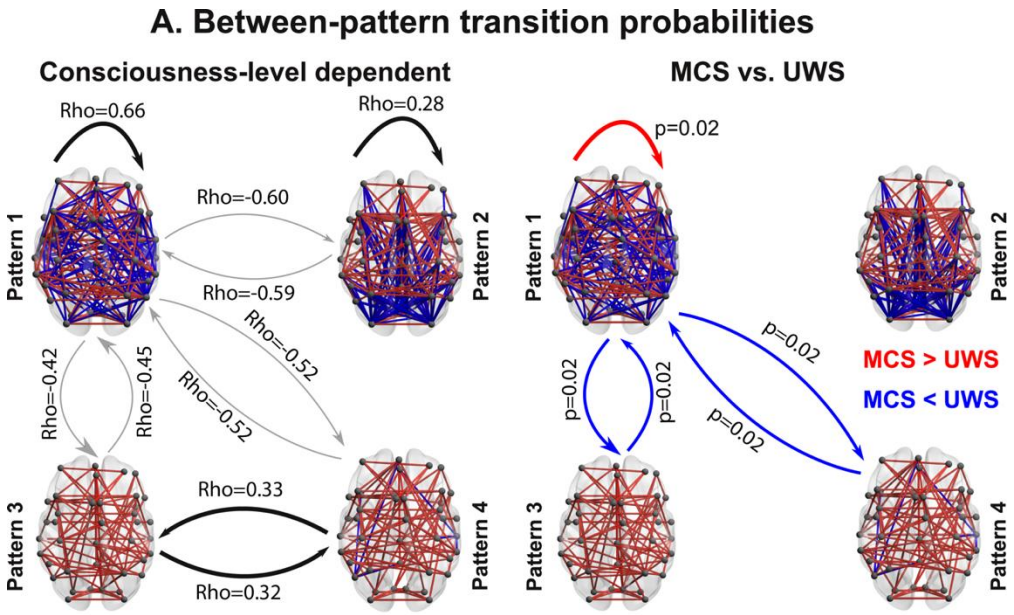

Fig. S7. Transition probabilities normalized by the patterns' probabilities of occurrence. The analysis in Figure 2A is replicated subtracting for each participant the corresponding null-model transition probability matrix, as obtained by surrogate state sequences that are randomly shuffled versions of the original sequences.

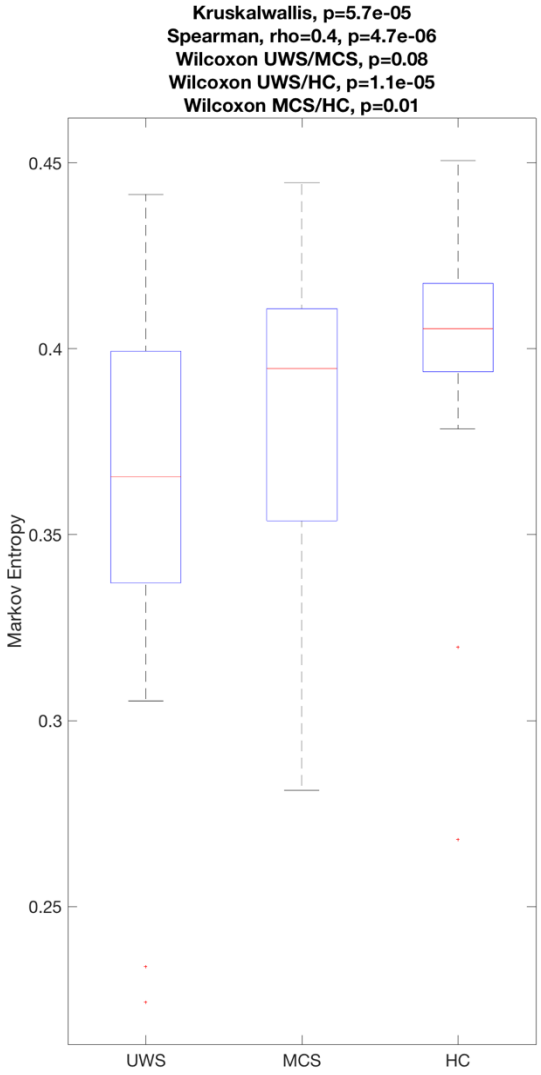

Fig. S8. Entropy rate increases with respect to the state of consciousness. For each participant, the predictability of the dynamic sequence of patterns was quantified using the entropy rate (i.e. Markov entropy). The entropy rate was computed from the corresponding patterns' probabilities and the transition probability matrices. Sequence predictability decreased systematically with the individuals' state of consciousness.

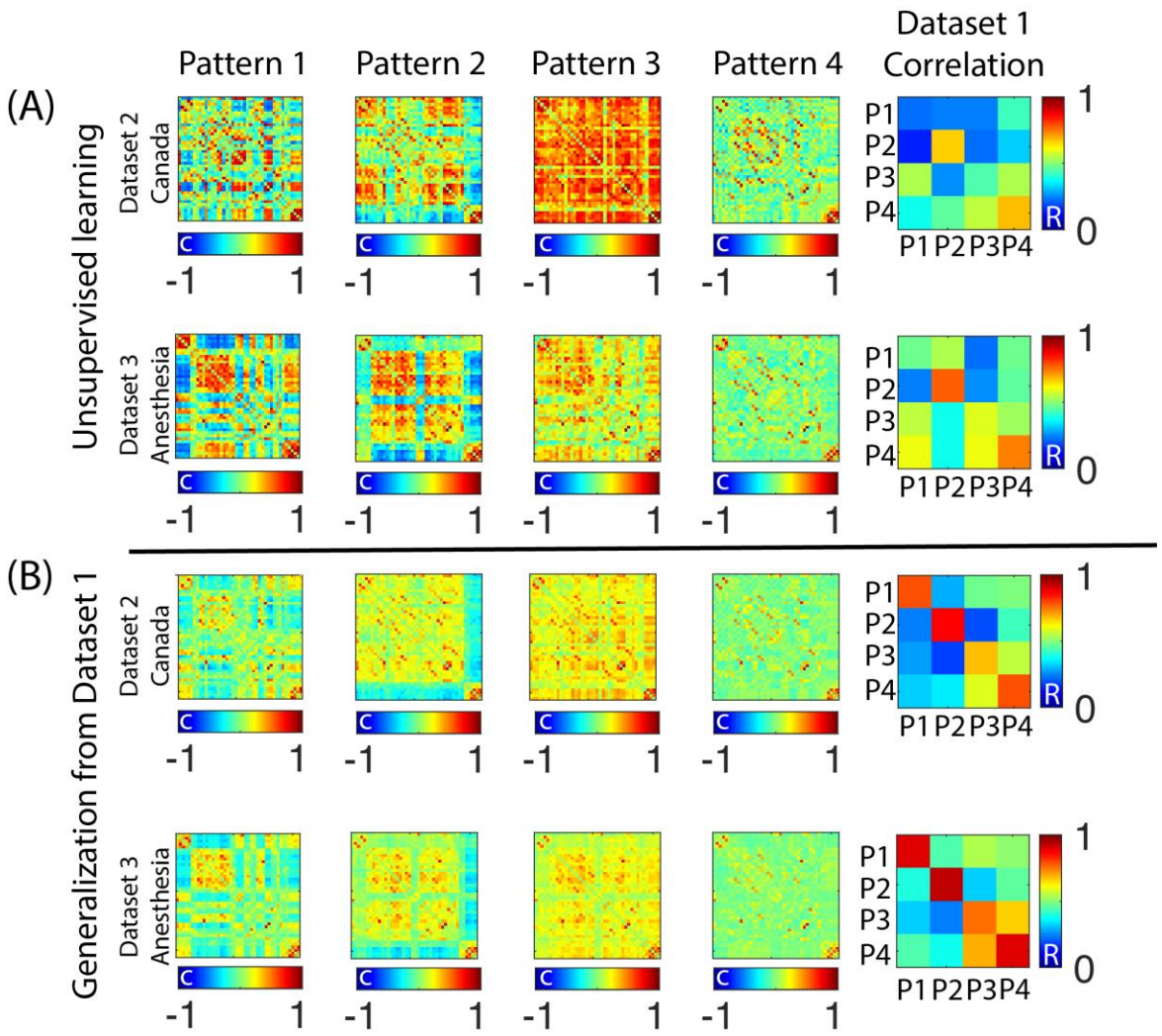

Fig. S9. Pattern validation in dataset 2 ("Canada") and dataset 3 ("Anesthesia"). To verify the validity of the identified patterns in these datasets, we performed the following two analyses. (**A**) First, we replicated the unsupervised learning (k-means clustering) used in dataset 1 (Figures 1 and S4) in datasets 2 and 3. The obtained patterns are shown in the left panel and the similarity (Pearson's linear correlation coefficient) of these patterns with respect to those from dataset 1 are shown in the right panel. Note that the unsupervised learning method (k-means clustering) can yield suboptimal results when the number of samples / observations is low relative to the number of features / dimensions. Because of this, the patterns are likely affected by the smaller number of participants included in datasets 2 and 3 vs. dataset 1 (n=125 in dataset 1, n=11 in dataset 2 and n=23 in dataset 3). (**B**) As performed in the main manuscript, we first applied a unsupervised method based on pattern detection in dataset 1 via k-means, and on the subsequent labeling of each phase coherence matrix in datasets 2 and 3 according to their distance to the centroids detected in dataset 1, i.e. each volume was assigned the label corresponding to the

centroid (as obtained in dataset 1) that was the closest to the phase coherence matrix at that volume. We then averaged the temporal series of phase coherence matrices that were assigned each label in datasets 2 and 3. The resulting average patterns are shown in the left panel. These patterns present a high similarity to the patterns obtained from dataset 1, and then generalized to datasets 2 and 3 (right panel).

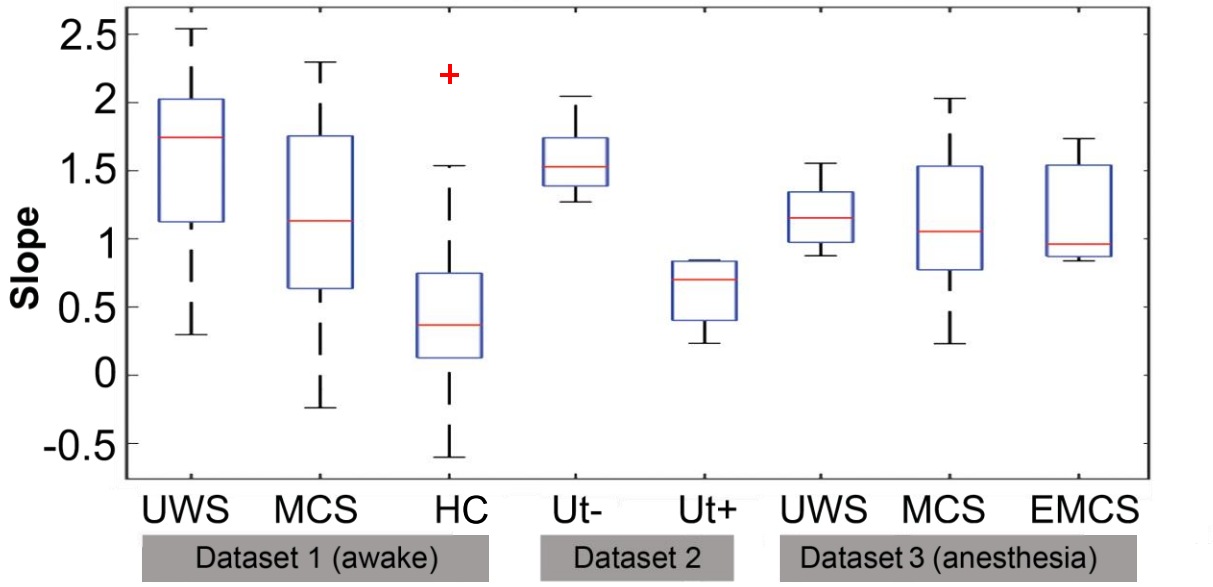

	MCS awake	Healthy awake	Ut-	Ut+	UWS anesth	MCS anesth	EMCS anesth
UWS awake	0.0071	1.6e-10*	0.73	0.0034*	0.0640	0.01	0.2
MCS awake		2.2e-06*	0.15	0.076	0.96	0.73	0.98
Healthy awake			2.5e-04*	0.34	0.0014*	3.5e-04*	0.03*
Ut-				0.0043*	0.026*	0.091	0.26
Ut+					0.0043*	0.087	0.071
UWS anesth						0.71	0.71
MCS anesth							0.86

Fig. S10. Dataset slope comparisons. ***top*** Datasets are compared with respect to the slopes representing the relationship between rates of pattern occurrence and corresponding functional-structural similarity. The slopes are displayed for each group across all datasets. ***bottom*** Between-group statistical comparisons (p: Wilcoxon rank sum test values).

Notes: UWS: unresponsive wakefulness syndrome (17 awake, 6 anesthetized), MCS: minimally conscious state (23 awake, 14 anesthetized), HC: healthy controls (21 awake), EMCS: emergence from the MCS (3 anesthetized), Ut-: unresponsive patients who do not show command following on mental imagery tasks (6 awake), Ut+: non-behavioral minimally conscious state/cognitive-motor dissociation (5 awake). Boxplots represent medians with interquartile range and maximum-minimum values (whiskers).

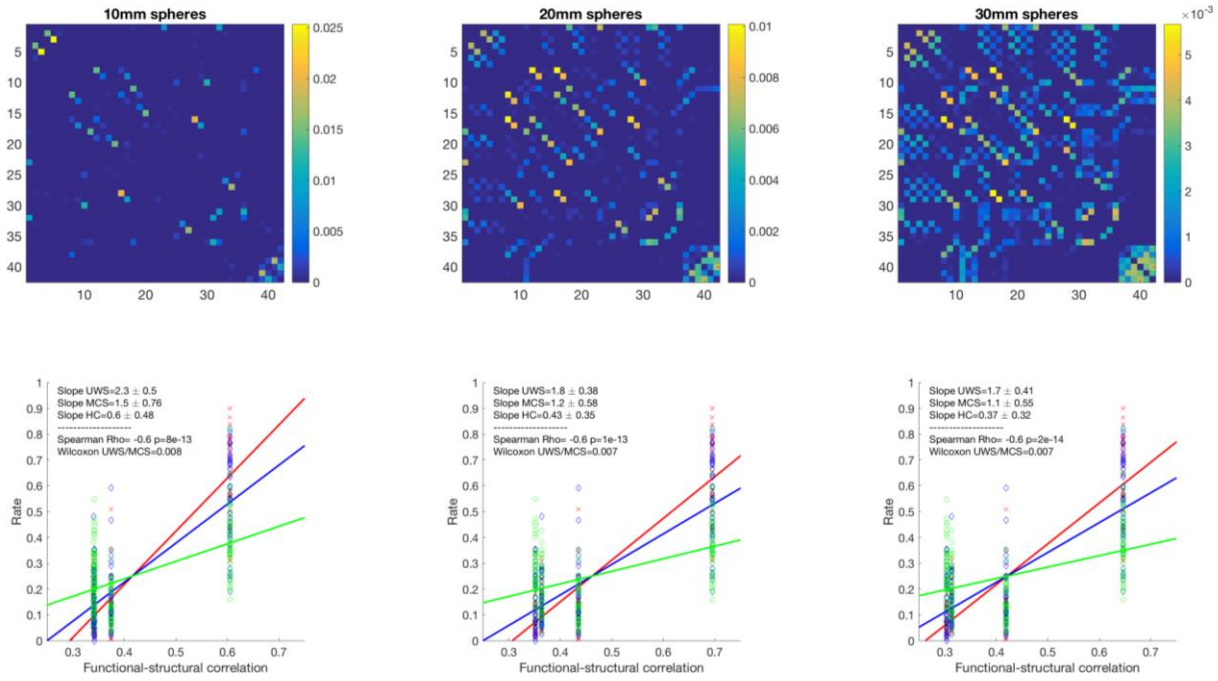

Fig. S11. Replication of the structural-functional analysis with different granularity of the structural matrix reduction. The original DSI matrix was reduced to the functional ROIs using either spheres of 10 mm (left panel), 20 mm (middle panel) and 30 mm (right panel). In all cases similar results were obtained for the slopes characterising the probability of the patterns and their corresponding functional-structural correlation (bottom panels). 30 mm spheres were used in all other analyses in this work.

Table S1. Patients' demographic and clinical characteristics per scanning site (*n* = 112).

							Coma Recovery Scale-Revised						
DS	**Site**	**Diagnosis**	**Gender**	**Age at scan**	**Etiology**	**Days since injury**	**Auditory function**	**Visual function**	**Motor function**	**Oromotor/Verbal function**	**Communi-cation**	**Arousal**	**#CRS-R assessments**
1	Liège	MCS	F	34	1	3034	3	3	2	2	0	2	5
1	Liège	MCS	M	62	2	13	0	3	2	1	0	1	6
1	Liège	MCS	F	59	3	21	1	3	2	0	0	2	7
1	Liège	MCS	M	30	1	246	3	2	2	2	0	1	3
1	Liège	MCS	M	83	3	13	3	0	2	1	0	0	5
1	Liège	MCS	M	34	3	1077	3	5	2	0	1	1	4
1	Liège	MCS	M	52	3	20	3	3	2	2	1	2	4
1	Liège	MCS	M	47	1	533	3	5	2	1	0	2	13
1	Liège	MCS	M	38	3	1854	1	3	2	2	0	1	4
1	Liège	MCS	M	29	3	64	1	3	2	1	0	2	2
1	Liège	MCS	M	41	2	9900	3	3	2	2	0	2	8
1	Liège	MCS	M	23	1	301	1	3	2	1	0	2	6

1	Liège	MCS	M	53	2	1241	0	3	2	2	0	2	5
1	Liège	MCS	F	46	3	242	1	3	2	1	0	1	7
1	Liège	MCS	M	60	1	15	3	5	5	3	1	1	1
1	Liège	MCS	M	61	1	135	3	4	2	1	0	2	7
1	Liège	MCS	M	68	1	360	0	3	2	0	0	2	3
1	Liège	MCS	M	35	1	1331	3	0	2	1	0	2	10
1	Liège	MCS	F	48	1	291	2	1	2	2	0	1	8
1	Liège	MCS	M	73	3	35	0	2	0	1	0	1	3
1	Liège	MCS	M	23	1	645	3	3	0	1	0	2	8
1	Liège	MCS	M	11	2	1482	3	4	2	2	1	2	9
1	Liège	MCS	M	66	1	674	3	0	1	2	0	1	5
1	Liège	UWS	F	52	3	283	1	0	2	2	0	1	8
1	Liège	UWS	M	36	2	6709	1	0	2	1	0	2	6
1	Liège	UWS	M	30	2	743	1	0	2	1	0	2	7
1	Liège	UWS	M	74	2	92	1	0	1	1	0	1	9
1	Liège	UWS	F	44	2	8	0	0	1	0	0	1	4
1	Liège	UWS	M	67	3	43	1	0	2	1	0	1	5
1	Liège	UWS	M	63	2	30	1	1	2	2	0	2	1
1	Liège	UWS	M	31	1	849	1	1	2	1	0	2	11
1	Liège	UWS	M	87	3	7	0	0	2	1	0	1	1
1	Liège	UWS	F	41	2	1572	1	0	1	1	0	2	8
1	Liège	UWS	F	50	2	38	0	0	0	2	0	1	3

1	Liège	UWS	M	44	2	27	1	0	1	0	0	2	1
1	Liège	UWS	F	16	2	27	1	0	1	1	0	1	6
1	Liège	UWS	F	49	2	129	1	0	0	1	0	2	5
1	Liège	UWS	M	36	2	2031	1	0	1	2	0	2	6
1	Liège	UWS	M	34	2	7814	1	0	1	1	0	2	5
1	Liège	UWS	F	49	2	277	1	0	2	2	0	1	5
1	NY	MCS	F	56	3	1004	Diagnosis on clinical consensus						NA
1	NY	MCS	F	24	3	645	3	3	2	0	0	1	1
1	NY	MCS	F	57	3	1722	4	3	5	0	0	2	2
1	NY	MCS	F	58	2	373	2	3	5	2	0	2	1
1	NY	MCS	F	27	1	1719	3	4	5	1	0	2	1
1	NY	MCS	M	39	3	1410	0	2	4	0	0	2	4
1	NY	MCS	F	59	1	4564	1	1	2	0	0	2	5
1	NY	MCS	M	26	1	3366	1	3	2	1	0	2	4
1	NY	MCS	F	27	2	2049	2	3	1	2	0	2	4
1	NY	MCS	M	55	1	1896	3	4	5	2	0	2	5
1	NY	UWS	M	40	2	2097	1	1	2	1	0	1	2
1	NY	UWS	M	39	1	1660	1	1	2	0	0	1	2
1	NY	UWS	F	24	1	982	1	0	1	0	0	2	1
1	NY	UWS	M	38	1	1960	0	0	0	0	0	2	2
1	NY	UWS	M	53	2	1132	1	0	2	0	0	2	3
1	NY	UWS	M	27	1	1948	0	1	2	0	0	2	9

1	Paris	MCS	M	66	2	96	3	2	2	3	1	2	1
1	Paris	MCS	F	38	2	7	1	3	2	1	0	2	2
1	Paris	MCS	M	74	1	62	2	3	2	1	0	1	2
1	Paris	MCS	M	54	2	260	3	1	5	2	1	2	1
1	Paris	MCS	M	44	2	50	3	3	3	1	0	2	2
1	Paris	MCS	M	20	1	62	3	3	5	1	0	2	2
1	Paris	MCS	M	26	3	78	1	3	3	1	0	2	2
1	Paris	MCS	F	63	2	65	1	3	2	1	0	1	2
1	Paris	MCS	M	68	3	49	3	3	3	1	0	2	1
1	Paris	UWS	M	22	2	96	1	0	1	1	0	2	2
1	Paris	UWS	M	25	2	17	2	0	2	1	0	1	2
1	Paris	UWS	M	24	1	90	1	1	0	1	0	1	1
1	Paris	UWS	F	49	2	81	1	2	1	2	0	2	1
1	Paris	UWS	F	48	3	33	1	2	2	1	0	1	2
1	Paris	UWS	M	34	1	41	1	1	2	1	0	1	2
1	Paris	UWS	M	26	2	65	1	0	1	2	0	1	2
1	Paris	UWS	F	36	3	31	1	0	2	1	0	1	2
1	Paris	UWS	F	52	2	45	1	0	2	1	0	2	2
1	Paris	UWS	M	25	1	2178	1	1	2	2	0	2	1
1	Paris	UWS	F	29	3	1651	0	0	1	1	0	1	2
1	Paris	UWS	M	47	3	16	1	0	1	1	0	1	1
1	Paris	UWS	M	67	2	193	0	1	1	1	0	1	2

2	Lond Ont	Ut+	M	38	1	4552	1	0	2	1	0	2	21
2	Lond Ont	Ut+	F	44	1	7446	0	1	0	0	0	2	11
2	Lond Ont	Ut+	F	35	2	739	0	0	2	1	0	2	5
2	Lond Ont	Ut+	M	19	2	75	2	1	1	1	0	2	4
2	Lond Ont	Ut+	F	51	2	326	1	0	1	1	0	1	6
2	Lond Ont	Ut-	M	57	2	1129	1	1	2	1	0	1	7
2	Lond Ont	Ut-	F	20	3	2051	1	1	1	1	0	2	5
2	Lond Ont	Ut-	F	43	2	1674	1	0	2	1	0	1	7
2	Lond Ont	Ut-	M	20	2	1455	1	1	0	1	0	2	5
2	Lond Ont	Ut-	F	52	2	2380	1	0	2	1	0	1	5
2	Lond Ont	Ut-	F	14	2	903	1	0	2	1	0	1	5

3	Liège	EMCS	F	34	1	418	4	5	6	3	2	3	9
3	Liège	EMCS	M	29	1	2424	3	5	6	3	1	3	6
3	Liège	EMCS	M	18	1	429	3	4	4	1	2	1	8
3	Liège	MCS	M	57	1	189	1	0	2	2	0	1	13
3	Liège	MCS	M	24	1	2690	3	3	2	0	0	2	12
3	Liège	MCS	M	23	1	421	3	3	3	1	1	2	5
3	Liège	MCS	M	29	1	244	1	3	2	2	0	1	6
3	Liège	MCS	M	60	2	722	3	1	1	1	0	2	5
3	Liège	MCS	F	29	3	745	0	2	1	1	0	2	8
3	Liège	MCS	F	55	1	202	3	4	5	2	0	2	8
3	Liège	MCS	M	22	1	2977	2	3	5	2	0	1	6
3	Liège	MCS	M	52	1	57	4	5	5	1	0	2	4
3	Liège	MCS	M	22	1	1108	1	2	1	1	0	2	7
3	Liège	MCS	M	63	3	18	1	1	5	3	1	1	4
3	Liège	MCS	M	26	1	2129	3	0	2	2	0	2	6
3	Liège	MCS	F	30	1	599	0	2	1	2	0	1	8
3	Liège	MCS	F	30	2	2411	3	3	1	1	0	2	7
3	Liège	UWS	M	26	3	235	0	0	2	1	0	1	5
3	Liège	UWS	F	53	3	24	1	0	2	1	0	1	2
3	Liège	UWS	M	41	1	419	0	1	1	1	0	2	6
3	Liège	UWS	M	48	1	52	1	0	1	1	0	2	8
3	Liège	UWS	M	25	1	722	1	0	2	1	0	1	11

3	Liège	UWS	M	46	3	1113	1	0	1	0	0	1	6

DS=Dataset Dataset 1,2: patients scanned in sedation-free condition**;** dataset 3: patients scanned under propofol anesthesia

Diagnosis: MCS: minimally conscious state, UWS: vegetative state/ unresponsive wakefulness syndrome, EMCS: emergence from the minimally conscious state, Ut+: behaviorally unresponsive wakefulness syndrome showing command following only on mental imagery tasks, alternatively known as cognitive-motor dissociation, Ut-: behaviorally vegetative state/ unresponsive wakefulness syndrome not showing command-following on mental imagery tasks.

Etiology: 1: traumatic brain injury, 2: anoxia, 3: other

Coma Recovery Scale-Revised subscales (*denotes MCS, †denotes emergence from MCS)

- **Auditory function** 4: Consistent Movement to Command*, 3: Reproducible Movement to Command*, 2: Localization to Sound, 1: Auditory Startle, 0: None
- **Visual function** 5: Object Recognition*, 4: Object Localization: Reaching*, 3: Visual Pursuit*, 2: Fixation*, 1: Visual Startle, 0: None
- **Motor function** 6: Functional Object Use†, 5: Automatic Motor Response*, 4: Object Manipulation*, 3: Localization to Noxious Stimulation*, 2: Flexion Withdrawal, 1: Abnormal Posturing, 0: None/Flaccid
- **Oromotor/Verbal function** 3: Intelligible Verbalization*, 2: Vocalization/Oral Movement, 1: Oral Reflexive Movement, 0: None
- **Communication scale** 2: Functional: Accurate†, 1: Non-Functional: Intentional*, 0: None
- **Arousal scale** 3: Attention, 2: Eye Opening without stimulation, 1: Eye Opening with stimulation 0: Unarousable

Table S2. Network-level ROIs used as seed areas. The regions were defined as 10mm-diameter spheres around peak x,y,z coordinates selected from the literature.

Intrinsic connectivity network	Brodmann area [centered at x, y, z]
Default mode network	
Posterior cingulate cortex/precuneus	31 [0 -52 27]
Medial prefrontal cortex	9 [-1 54 27]
Lateral parietal cortex [left] [right]	39 [-46 -66 30] [49 -63 33]
Inferior temporal cortex [left] [right]	21 [-61 -24 -9] [58 -24 -9]
Frontoparietal network	
Dorsolateral prefrontal cortex [left] [right]	9 [-43 22 34] [43 22 34]
Inferior parietal lobule [left] [right]	40 [-51 -51 36] [51 -47 42]
Premotor cortex left [left] [right]	6 [-41 3 36] [41 3 36]
Midcingulate cortex	23 [0 -29 30]
Angular gyrus [left] [right]	39 [-31 -59 42] [30 -61 39]
Salience	
Orbital frontoinsula [left] [right]	12 [-40 18 -12] [42 10 -12]
Temporal pole [left] [right]	38 [-52 16 -14] [52 20 -18]
Paracingulate	32 [0 44 28]
Dorsal anterior cingulate	24 [-6 18 30]
Supplementary motor area [left] [right]	6 [-4 14 48] [4 14 48]
Parietal operculum [left] [right]	40 [-60 -40 40] [58 -40 30]
Ventrolateral prefrontal cortex	47 [42 46 0]
Dorsolateral prefrontal cortex [left] [right]	46 [-38 52 10] [30 48 22]
Auditory	
Superior transverse temporal gyrus [left] [right]	41/42 [-44 -6 11] [44 -6 11]
Precentral gyrus [left] [right]	6 [-53 -6 8] [58 -6 11]
Anterior cingulate cortex	24 [6 -7 43]
Sensorimotor	
Primary motor cortex [left] [right]	3 [-39 -26 51] [38 -26 48]
Supplementary motor area	[0 -21 48]
Visual	

Primary visual cortex [left] [right]	17 [-13 -85 6] [8 -82 6]
Secondary visual cortex [left] [right]	18 [-6 -78 -3] [6 -78 -3]
Associative visual cortex [left] [right]	19 [-30 -89 20] [30 -89 20]